ELSEVIER

Physica B 249–251 (1998) 775–779

PHYSICA B

Low-temperature conduction and giant negative magnetoresistance in III–V-based diluted magnetic semiconductor: (Ga, Mn)As/GaAs

A. Oiwa[a,*], S. Katsumoto[1,a], A. Endo[a], M. Hirasawa[a], Y. Iye[1,a], F. Matsukura[b], A. Shen[b], Y. Sugawara[b], H. Ohno[b]

[a] *Institute for Solid State Physics, University of Tokyo, Roppongi, Minato-ku, Tokyo 106, Japan*
[b] *Research Institute of Electrical Communication, Tohoku University, Katahira, Aoba-ku, Sendai 980-77, Japan*

Abstract

We have studied the transport and magnetic properties of $Ga_{1-x}Mn_xAs/GaAs$ with different Mn content ($0.015 < x < 0.071$) for temperatures 40 mK–250 K and magnetic fields 0–15 T. Ferromagnetic order was observed in the samples with $x > 0.02$. With incresing Mn concentration, the system undergoes an insulator–metal–insulator transition. Low temperature hopping conduction on the insulator side of the metal–insulator boundaries exhibits giant negative magnetoresistance.

Keywords: Diluted magnetic semiconductors; Ferromagnetism; Metal–insulator transition; Giant negative magnetoresistance

1. Introduction

The recent developments in the molecular beam expitaxy (MBE) technique have enabled us to grow III–V compound based diluted magnetic semiconductors such as $In_{1-x}Mn_xAs$ [1–3] and $Ga_{1-x}Mn_xAs$ [4–6] with high Mn content x. In the course of recent studies on $In_{1-x}Mn_xAs$ [1,2], $Ga_{1-x}Mn_xAs$ [4–6] and their related structures [3], it has been elucidated that the electrical transport properties are dramatically influenced by the exchange interaction between the conduction carriers and the localized moments. In the transport studies on Mn-doped GaAs carried out in the early days [7,8], bulk samples were used and the Mn concentration was limited to $x \leqslant 0.005$ and only an insulating behavior was observed. In this work, a series of samples of $Ga_{1-x}Mn_xAs$ with x ranging from 0.015 to 0.071 were grown and their magnetism and spin-dependent magnetotransport were investigated. The overall trend of changes as a function of x, including an insulator–metal–insulator

* Corresponding author. Tel.: + 81-3-3478-6811, ex. 5602; fax: + 81-3-3478-0536; e-mail: oiwa@kodama.issp.u-tokyo.ac.jp.

[1] Also at CREST, Japan Science and Technology Corporation (JST).

0921-4526/98/$19.00
PII: S0921-4526(98)00312-3

transition has been already reported [6]. In the present paper, we focus upon the giant negative magnetoresistance effect observed on the insulating side of the metal-insulator transitions.

2. Experimental

Samples studied in this work were grown by MBE at a relatively low substrate temperature. The low-temperature growth was essential in suppressing the segregation of Mn and enabled us to grow higher Mn concentration ($x \sim 0.07$) samples. A typical growth procedure [4,5] is as follows: firstly a GaAs layer about 100 nm thick was grown on a semi-insulating (1 0 0) GaAs substrate at a substrate temperature of 700°C. After lowering the substrate temperature to 250°C, a buffer layer of GaAs about 100 nm thick and a $Ga_{1-x}Mn_xAs$ layer about 150 nm thick were grown successively. Six samples of $Ga_{1-x}Mn_xAs$/GaAs which are numbered from #1 to #6 had Mn content, $x = 0.015$, 0.022, 0.035, 0.043, 0.053 and 0.071, respectively. The magnetization data for six samples were taken by using a commercial SQUID magnetometer. The electrical transport properties were measured at temperatures down to 40 mK under magnetic fields up to 15 T using a dilution refrigerator and a superconducting magnet. During the course of the transport measurements, we found considerable anisotropy within the (1 0 0) plane. To clarify the conductivity anisotropy, we patterned the samples by photolithography and wet etching into an L-shaped Hall bar as depicted in Fig. 4, so as to investigate the conduction in the [0 1 $\bar{1}$] and [0 1 1] directions separately.

3. Results and discussion

Ferromagnetic order is at low temperatures in all samples excepting #1. Fig. 1 shows the ferromagnetic transition temperatures for the six samples determined from the SQUID measurements. The ferromagnetic transition temperature becomes maximum (~ 70 K) around $x = 0.04$, and decreases with further increase of x. Fig. 2 shows the magnetization curves for the six samples at 2 K.

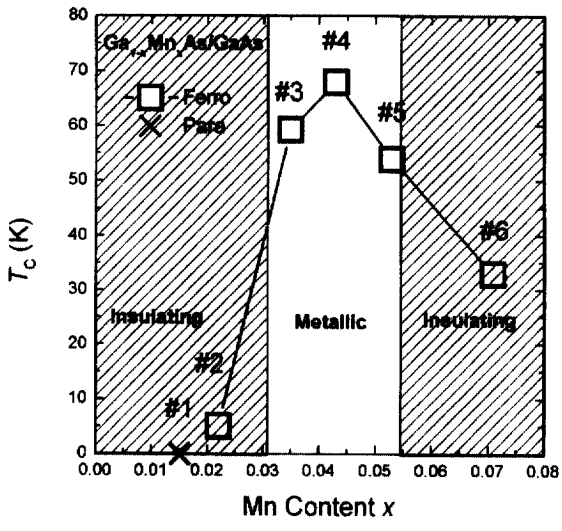

Fig. 1. Ferromagnetic transition temperature T_C as a function of Mn content x. T_C is determined from the magnetization curve measured using a SQUID magnetometer. Sample #1 remains paramagnetic down to the lowest temperature.

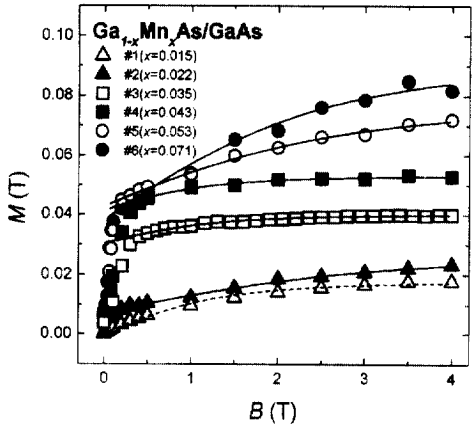

Fig. 2. Magnetization curves for six samples of $Ga_{1-x}Mn_xAs$/GaAs with x ranging from 0.015 to 0.071 at 2 K. The solid curves for samples #2 – #6 are the fits of the modified Brillouin function to the experimental data. The dashed curve for sample #1 represents the fit of the Brillouin function. The magnetic field is perpendicular to the sample plane for samples #3 – #6 and parallel to the plane for samples #1 and #2.

The direction of magnetic field was parallel to the sample plane for #1 and #2, and perpendicular for the rest. It should be mentioned that the low-field part of the magnetization curve is sensitive to

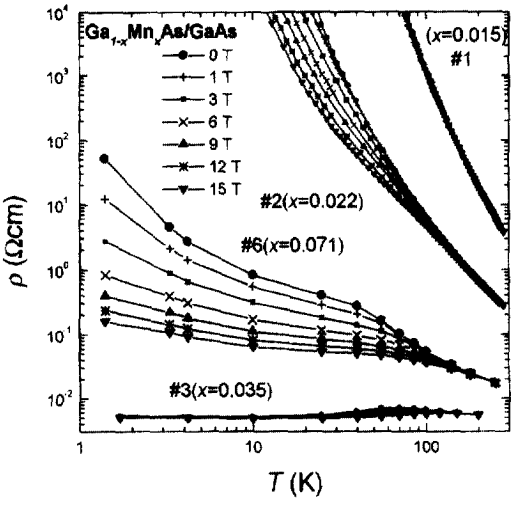

Fig. 3. Temperature dependence of resistivity for four samples of $Ga_{1-x}Mn_xAs/GaAs$ with x ranging from 0.015 to 0.071 at different magnetic fields.

the field orientation, but the high-field part near saturation is not. The magnetization curve of sample #1 can be fitted by a Brillouin function as shown by the dashed curve in Fig. 2. On the other hand in the ferromagnetic samples, the magnetization curve consists of two parts; one is the ferromagnetic component which saturates in the low-field region and the other is a component slowly increasing in the high-field region. In the insulating samples #2, #5 and #6 the slowly increasing component is large, while it is relatively small in metallic samples #3 and #4 but still it does not saturate at the highest field. These slowly increasing components are described by a modified Brillouin function shown by solid curves in Fig. 2 which phenomenologically takes account of antiferromagnetic interaction between the localized magnetic moments [9]. The saturation values of magnetization are in agreement with those estimated from $M_S = N_{Mn} g \mu_B S_{Mn}$ assuming $S_{Mn} = \frac{5}{2}$. This is consistent with an expectation that Mn ions are divalent and act as acceptors.

Fig. 3 shows the temperature dependence of resistivity at different magnetic fields for four samples with Mn content $x = 0.015, 0.022, 0.035, 0.071$. The presently studied range of x of $Ga_{1-x}Mn_xAs/GaAs$ can be divided into the three regimes bounded by two metal–insulator boundaries. The shaded regions in Fig. 1 are the insulating regime and the unshaded region represents the metallic one. Although we are mainly concerned with magnetotransport in the insulating regimes, it is worthwhile to briefly summarize the behavior in the metallic regime [6]. In the metallic regime, the temperature dependence of resistivity shows a characteristic peak at around T_C, and the magnitude of the negative magnetoresistance becomes maximum there, as can be seen for sample #3 in Fig. 3. The origins of the resistivity peak is attributed to the spin disorder scattering in the critical region [10]. The spin disorder scattering model also gives a good explanation for the negative magnetoresistance in the metallic samples [11,12].

On the insulating side of the metal–insulator transition boundaries, the negative magnetoresistance becomes much larger than in the metallic regime. Very large negative magnetoresistance is observed in samples #6 as well as #2 as seen in Fig. 3. In #6, the reduction of resistivity exceeds two orders of magnitude at 15 T and the lowest temperature. A broad hump is seen in the temperature dependence of the zero field resistivity of #6 near $T_C \sim 35$ K, which may be interpreted in terms of critical scattering as in the case of the metallic sample #3.

The behavior of sample #2 is similar to #6, although the experimental temperature range is limited by its faster increase of resistivity. The resistivity of sample #1 shows an activationtype temperature dependence. The activation energy for sample #1 is 75 meV, which is smaller than the value $\sim$ 110 meV quoted as an isolated Mn acceptor level from the edge of the valence band [7].

No significant magnetoresistance is observed for sample #1 in the measurable temperature range. Thus, it seems obvious that the giant negative magnetoresistance is a characteristic feature of the samples on the insulating side and in the vicinity of the metal–insulator transition. Referring to the magnetization data in Fig. 2, the emergence of giant negative magnetoresistance appears to be correlated with the slowly increasing component of the magnetization.

The giant negative magnetoresistance which continues up to high fields must result from the

presence of the magnetic exchange interaction between the carriers and the localized magnetic moments. We have proposed two possible scenarios for the giant negative magnetoresistance [6]. The first is the destruction of the bound magnetic polaron (BMP) which has been invoked earlier for $In_{1-x}Mn_xAs$ [2] and other material [13]. At zero field, a carrier is surrounded by a cloud of randomly oriented spins. This constitutes a magnetic polaron which is likely to be localized by disorder. When a high magnetic field is applied all Mn spins are progressively aligned to the direction of the applied magnetic field, which makes the carriers increasingly mobile. The disappearance of BMP may be correlated with the slowly increasing component of the magnetization curve.

The second scenario is based on Anderson localization [14]. In the variable hopping regime, the localization length ξ is a function of $(E_C - E_F)$, where E_F is the Fermi energy and E_C is the mobility edge. Application of magnetic field induces a shift of the mobility edge as well as the Zeeman shift of the Fermi energy, and makes $(E_C - E_F)$ of either of the up-spin or down-spin subband much smaller than at zero field, giving rise to a marked increase of ξ for that subband. The magnetic-field-induced shift of the mobility edge is due to reduction of spin disorder which is signaled by the gradual approach of the magnetization to saturation. Either of the two scenarios may be applicable as far as the negative magnetoresistance of sample #6 with $x = 0.071$ is concerned. However, the results for samples #1 with $x = 0.015$, and #2 with $x = 0.022$, seems to favor the second scenario, because the large negative magnetoresistance occurs only in the vicinity of the metal–insulator boundaries. It seems rather difficult to explain the abrupt change in magnetotransport behavior between samples #1 and #2 in the framework of the BMP model. On the other hand, it is natural in the Anderson localization scenario that the negative magnetoresistance should diminish when the system is deep in the insulating regime and E_F is far from E_C.

At temperatures below 1 K, the resistivity in the "re-entrant" insulating regime starts to show a very large anisotropy in their resistivity , i.e. there occurs a large difference in the value of the resistivity and

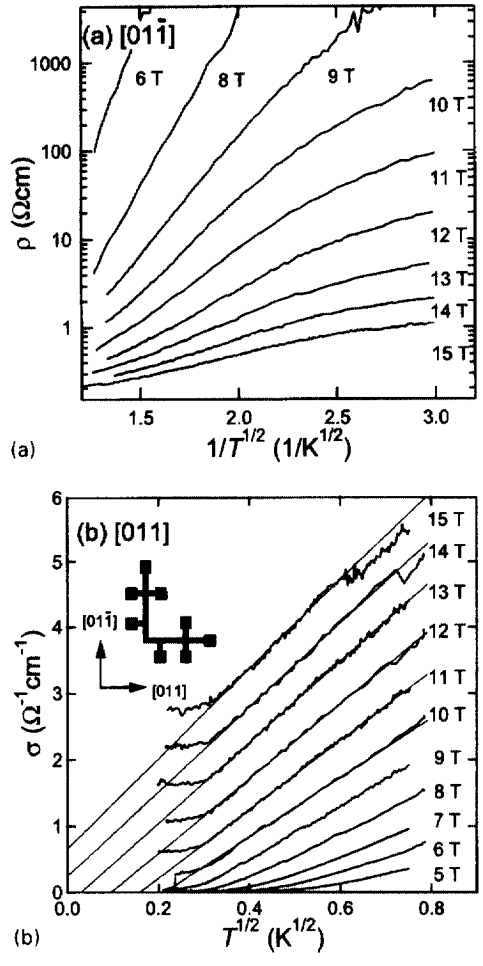

Fig. 4. Temperature dependence of resistivity for sample #6, $Ga_{0.929}Mn_{0.071}As/GaAs$ at low temperatures in different magnetic fields. (a) the resistivity measured in the [0 1 $\bar{1}$] direction plotted as $\log\rho$ verses $T^{-1/2}$, (b) the conductivity in the [0 1 1] direction plotted as σ vs $T^{1/2}$. The top figure shows the pattern of the L-shaped Hall bar used for this experiment.

its temperature dependence between the current along the [0 1 $\bar{1}$] and [0 1 1] directions. This in-plane anisotropy is unique in the re-entrant insulating regime, while in the lower Mn content regime rather than re-entrant regime the resistivity shows small or no in-plane anisotorpy even at low temperatures. Fig. 4 shows the transport behavior of sample #6 at temperatures lower than Fig. 3. For the current along the [0 1 $\bar{1}$] direction, which is the high resistivity direction, the resistivity shows

a variable-range-hopping-type temperature dependence down to $\sim$ 500 mK. In Fig. 4a, we plotted the resistivity data as $\log\rho$ verses $T^{-1/2}$, which is inspired by the Coulomb-gap-limited hopping model for strongly localized interacting electrons [15]. For the current parallel to the [0 1 1] direction, which is the low resistivity direction, the conductivity seems better described by $\sigma(T,H) = \sigma(0,H) + A(H)T^{1/2}$ as shown in Fig. 4b. Evidently, the conduction path in sample #6 is quite complicated and may consist of a parallel circuit of the low resistivity filaments. The structural origin of this in-plane anisotropy is presently unknown.

4. Summary

$Ga_{1-x}Mn_xAs$/GaAs undergoes an insulator–metal–insulator transition with increasing x. A giant negative magnetoresistance is observed in samples on the insulating side and near the metal–insulator boundaries. A scenario based on the Anderson localization is proposed as a mechanism of the negative magnetoresistance. The insulating sample with high Mn content exhibit a large difference in resistivity for the current along the [0 1 $\bar{1}$] and [0 1 1] direction below 1 K. Elucidation of the origin of such a strong in-plane anisotropy awaits further studies, particularly microstructural characterization.

Acknowledgements

This work is partly supported by a Grant-in-Aid for the Scientific Research on Priority Area "Spin Controlled Semiconductor Nanostructures" from the Ministry of Education, Science, Sports and Culture, Japan. The authors thank Professor H. Takagi at ISSP for his help with the SQUID measurements.

References

[1] H. Munekata, H. Ohno, S. von Molnar, A. Segmüller, L.L. Chang, L. Esaki, Phys. Rev. Lett. 63 (1989) 1849.
[2] H. Ohno, H. Munekata, T. Penny, S. von Molnar, L.L. Chang, Phys. Rev. Lett. 68 (1992) 2664.
[3] H. Munekata, A. Zaslavsky, P. Fumagalli, R.J. Gambino, Appl. Phys. Lett. 63 (1993) 2929.
[4] H. Ohno, A. Shen, F. Matsukura, A. Oiwa, A. Endo, S. Katsumoto, Y. Iye, Appl. Phys. Lett. 69 (1996) 363.
[5] F. Matsukura, A. Oiwa, A. Shen, Y. Sugawara, N. Akiba, T. Kuroiwa, H. Ohno, A. Endo, S. Katsumoto, Y. Iye, Appl. Surf. Sci. 113/114 (1997) 178.
[6] A. Oiwa, S. Katsumoto, A. Endo, M. Hirasawa, Y. Iye, H. Ohno, F. Matsukura, A. Shen, Y. Sugawara, Solid State Commun. 104 (1997) 209.
[7] R.A. Chapman, W.G. Hutchinson, Phys. Rev. Lett. 18 (1967) 443.
[8] D.A. Blakemore, J.S. Woodbury, Phys. Rev. B 8 (1973) 3803.
[9] D. Heiman, Y. Shapira, S. Foner, B. Khazai, R. Kershaw, K. Dwight, A. Wold, Phys. Rev. B 29 (1984) 5634.
[10] M.E. Fisher, J.S. Langer, Phys. Rev. Lett. 20 (1968) 665.
[11] S.J. Allen, Jr., N. Tabatabaie, C.J. Palmstrom, G.W. Hull, T. Sands, F. DeRosa, H.L. Gilchrist, K.C. Garrison, Phys. Rev. Lett. 62 (1989) 2309.
[12] F. Matsukura, H. Ohno, A. Shen, Y. Sugawara, in preparation.
[13] S. von Molnar, J. Flouquet, F. Holtzberg G. Remenyi, Phys. Rev. Lett. 51 (1983) 706, and Solid State Electron. 28 (1985) 127.
[14] H. Fukuyama, K. Yosida, J. Phys. Soc. Japan 46 (1979) 102.
[15] B.L. Shklovskii, A.L. Efros, Electronic Processes in Doped Semiconductors, Springer, Berlin, 1984.